

Fast three dimensional migration of He clusters in bcc Fe and Fe–Cr alloysD. Terentyev,^{1,a)} N. Juslin,² K. Nordlund,² and N. Sandberg³¹*SCK-CEN, Nuclear Materials Science Institute, Boeretang 200, B-2400 Mol, Belgium*²*Department of Physics, EURATOM-Tekes, University of Helsinki, P.O. Box 43, FI-00014 Helsinki, Finland*³*Department of Neutron Research, Uppsala University, S-75121 Uppsala, Sweden and Division of Reactor Physics, Royal Institute of Technology, SE-10044 Stockholm, Sweden*

(Received 18 December 2008; accepted 4 April 2009; published online 20 May 2009)

In this work, we perform atomistic molecular dynamics simulations to assess the properties of small helium vacancy (He-V) and pure He clusters in body-centered cubic Fe and in Fe₉₀–Cr₁₀ (Fe–10Cr) random alloy. The following two goals are pursued: determining diffusion mechanisms of He-V clusters occurring in dynamic simulations and revealing a possible influence of Cr on the mobility/stability of He-V clusters in the Fe–10Cr alloy. We also present a newly developed set of interatomic potentials for the Fe–Cr–He system, fitted to a set of specially performed density functional theory calculations. The obtained results show that the dissociation energies of the studied He-V clusters, as well as the migration energy of He interstitial, are not significantly affected in the alloy compared to pure Fe. It was found that small pure He clusters with sizes up to four atoms, that were assumed to be immobile in many previous studies devoted to He-release/accumulation kinetics, in fact, exhibit fast three dimensional motion with a migration energy of tens of meV. The presence of 10% Cr in the Fe matrix, however, retards their mobility. We discuss possible reasons for the decreased diffusivity of these He clusters in the Fe–Cr alloy. © 2009 American Institute of Physics.

[DOI: 10.1063/1.3126709]

I. INTRODUCTION

Fe–Cr ferritic steels serving as or being candidate structural materials in present and future nuclear reactors are subject to intensive neutron irradiation during the working cycle. Fast neutrons have a high cross section to enter (n, α) transmutation reactions wherein helium is produced.¹ The production of large amounts of insoluble He is a special issue for the fusion environment and therefore an important problem in the design of fusion reactors.

Earlier and recent experiments have clearly shown that the evolution of microstructure is significantly affected in the presence of helium^{2–6} (and references therein). In general, it is accepted that helium atoms are deeply trapped at vacancies and their small clusters, which decreases vacancy mobility and enhances void nucleation. Enhanced void swelling and formation of He gas bubbles, in turn, leads to a dimensional instability and degradation of the mechanical properties of pure metals, model binary alloys, and real steels^{7–9} (and references therein). It should be noted that alloying of Fe by Cr affects the kinetics of He bubble nucleation and growth, as well as the diffusivity of nanometric bubbles, as directly observed using transmission electron microscopy.¹⁰ Therefore, it is not only important to rationalize how the accumulation of He and its redistribution occurs in body-centered cubic (bcc) Fe but also to reveal the possible role of Cr, the main alloying element in ferritic martensitic steels. This is the first step toward an understanding of He behavior in concentrated Fe–Cr alloys and industrial steels.

Atomistic simulations such as molecular static (MS), molecular dynamics (MD), and density functional theory cal-

culations (DFT) have already provided a substantial amount of information on solution and migration properties of He and He-vacancy (henceforth He-V) clusters in pure bcc Fe (see Refs. 11–15 and references therein). It has been shown that an isolated He atom occupying a tetra- or octahedral position, depending on the model, has an extremely low migration energy (~ 0.06 – 0.08 eV) in the bcc Fe lattice and is expected to execute fast three dimensional (3D) motion.^{16,17} The mobility of helium atoms is reduced drastically in the vicinity of defects, so He exhibits strong attractive interaction with vacancies with the binding energy, $E_b \sim 1.5$ eV, and weaker interaction with self-interstitial atoms (SIA) with $E_b \sim 0.3$ eV.^{15,17} Interstitial He atoms also exhibit relatively weak attractive interaction with each other.^{12,15} However, He clusters containing more than four atoms are expected to be unstable, being capable of emitting a self-interstitial atom.¹⁵

Modern large scale coarse grain models such as rate theory or kinetic Monte Carlo (KMC) methods applied to study evolution of damage in the presence of He heavily utilize the data obtained from atomistic simulations, as many basic migration properties cannot be extracted directly from experiment. However, due to the size limitations of the DFT approach or inaccuracy of the previously developed (not fitted to DFT data) interatomic potentials (IAPs), some important information about properties of He-defect complexes is still missing. As has recently been pointed out in Ref. 18, a number of important details related to the mobility and dissociation of small He-V clusters is overlooked in the existing object KMC (Ref. 19) and lattice KMC (Ref. 20) approaches. In particular, most of the existing models usually assume that all pure He and He-V clusters are immobile. A recent lattice KMC (LKMC) study has, however, shown that some small He-V clusters may exhibit significant mobility at elevated temperature thus also contributing to the growth of

^{a)}Author to whom correspondence should be addressed. Electronic mail: dterenty@sckcen.be.

large He bubbles. However, due to the limitations of the LKMC technique only vacancy rich He-V clusters were studied in Ref. 18, whereas the properties of He-rich and pure He clusters remain unexplored.

In this work, we perform atomistic calculations to assess the properties of He-V and pure He clusters in pure Fe and in Fe₉₀-Cr₁₀ (Fe-10Cr) alloy. We developed a new set of IAPs for Fe-He and Cr-He systems, especially fitted to a set of DFT calculations. The potential functional and parameter set are given in Appendix A. To describe the Fe-Cr system, we have opted for the two band model potential developed in Ref. 21, which was extensively used in the past few years to model Fe-Cr system (e.g., Ref. 21–25). The Fe-Fe part of this potential is the one derived by Ackland *et al.* in 2004,²⁶ which essentially is a refit of the “Mendelev” potential,²⁷ known to be significantly improved compared to the previously existing Fe-Fe many-body potentials in terms of description of self-interstitial defects and dislocation properties.^{28,29}

The set of the IAPs for Fe-Cr-He system was implemented in the existing MD codes DYMOKA (Ref. 30) and PARCAS (presented in Ref. 31) to perform both static and dynamic simulations. MS techniques were used to calculate formation energies of different He-V clusters and to provide the comparative diagram of the dissociation energy versus He density in the clusters, whereas MD simulations were used to study the motion of pure He and He-V clusters and their lifetimes. Note that MD modeling of the He-V cluster dissociation and measurement of related lifetimes is of practical interest and good verification of the data which otherwise could be obtained by static calculations. Thus, the goal of this work is twofold: (i) to investigate the possible mechanisms of motion of He-rich He-V clusters and (ii) to reveal a possible effect of Cr on the mobility and stability of He-V clusters in the Fe-10Cr random alloy. The choice of the Cr concentration was governed by two reasons: firstly, this composition corresponds to a typical Cr content in real ferritic martensitic steels; secondly, Fe-Cr alloys containing about 10% Cr do not yet exhibit α - α' phase separation or Cr ordering,³² so the random distribution of Cr atoms is physically justified.

II. SIMULATION TECHNIQUE

MS and MD calculations were performed using the DYMOKA (Ref. 30) and PARCAS (Ref. 31) codes, where the above-mentioned IAPs were implemented. Simulations were performed in bcc Fe and Fe-10Cr random alloy. Details of the applied IAPs and MS simulations are given in Appendices A and B, respectively. The size of the crystallite used in MD simulations was $10 \times 10 \times 10 a_0^3$, thus it contained 2000 atoms before a He-V cluster was introduced. Periodic boundary conditions were applied. The MD time step was variable in the range of 0.1–1.5 fs, determined by the fastest atom in the system. The equilibrium lattice constant a_0 for Fe and Fe-10Cr alloys was obtained from the “zero pressure” condition in the separate set of MD runs performed in the temperature range of 100–1800 K. The obtained data are presented in Fig. 1. All MD simulations were performed using

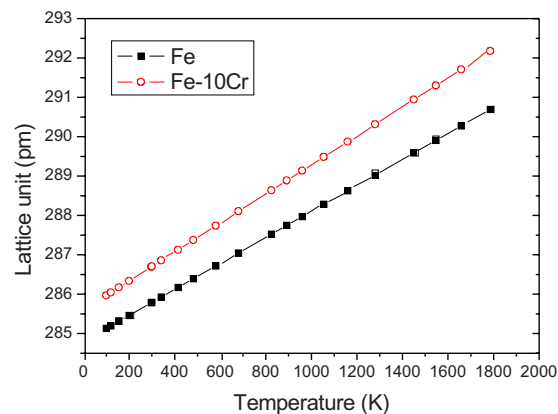


FIG. 1. (Color online) Temperature dependence of the equilibrium lattice constant for bcc Fe and random Fe-10Cr alloy.

classical MD in the microcanonical (NVE) ensemble, after equilibration of the crystallite to a given temperature within 10 ps.

Estimation of the binding and dissociation energies for He-vacancy clusters (henceforth $\text{He}_N\text{-V}_M$, where N and M denote the corresponding number of He atoms and vacancies forming a cluster) requires calculation of the formation energy of these clusters and corresponding migration energies of dissociating species, i.e., a He atom or vacancy. Definitions and methodology to calculate the formation energies of $\text{He}_N\text{-V}_M$ clusters in Fe and Fe-10Cr alloy are described in Appendix B. The corresponding binding energy of a vacancy and He to a He-V cluster was then estimated as¹¹

$$E_b(\text{V}) = E_f(\text{V}) + E_f(\text{He}_N\text{V}_{M-1}) - E_f(\text{He}_N\text{V}_M), \quad (1)$$

$$E_b(\text{He}) = E_f(\text{He}) + E_f(\text{He}_{N-1}\text{V}_M) - E_f(\text{He}_N\text{V}_M). \quad (2)$$

The formation energies of an isolated vacancy and He in the tetrahedral position were estimated to be 1.72 and 4.39 eV in pure Fe. In the case of Fe-10Cr alloys, again a set of calculations when a vacancy or He atom was introduced in different positions in the Fe-10Cr crystallite was performed to estimate the mean values, for details see Appendix B. The dissociation energy was then determined as a sum of the corresponding binding and migration energies of a species which leaves a He-V cluster.¹⁵ The migration energy of a vacancy and interstitial He atom in pure Fe was estimated using MS technique by dragging a defect between two equilibrium positions and finding the saddle point energy. In the Fe-10Cr alloy these migration energies were estimated using MD simulations by tracing the trajectory of a defect, calculating the diffusion coefficient, and constructing the corresponding Arrhenius plot.

We then performed MD simulations to study the stability and mobility of He-V clusters at finite temperature. It should be noted that the mobility of the most stable He-V clusters, those with He/V ratio ~ 1 , is expected to be governed by the mobility of vacancies, thus its direct study using classical MD technique is restricted due to the limitations of the physical time accessible in this method. Given that the presence of He atoms inside a vacancy cluster further decreases its mobility, it is not surprising that the most stable clusters

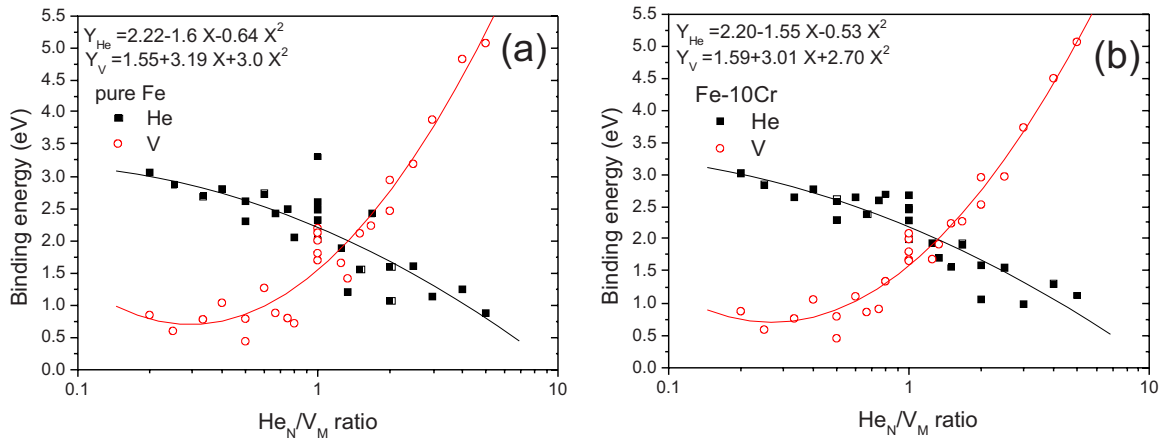


FIG. 2. (Color online) The binding energy of He-V clusters versus He/V ratio estimated using MS techniques in the pure Fe and Fe–10Cr alloy.

were seen to be practically immobile at low temperature and break apart before covering any substantial distance at high temperature. Here, the study is focused on the clusters with He/V ratio higher than 1, since we expected them to exhibit relatively high diffusivity, occurring mainly due to the motion of He interstitial atoms. Thus, we have considered pure He clusters with size up to four and some clusters containing vacancies such as He₂-V₁, He₃-V_{1,2}, and He₄-V_{1,2,3}. Pure He clusters with size larger than four atoms were not considered here, as it is expected that they are unstable against spontaneous emission of self-interstitial atom and spontaneously transform into He₅-V₁ cluster.¹⁵ In addition, we have considered one vacancy rich cluster, namely, He₂V₃, as we expected that its diffusivity could be measurable at high temperature even within the limited MD time scale.

Once a He-V cluster was introduced in the perfect bcc Fe or Fe–10Cr crystal, its coordinates and structure were traced during the MD run by identifying vacancies and interstitial atoms using the Wigner Seitz (WS) cell method and by following positions of He atoms every ten MD steps. This allows to detect the displacement of a cluster to follow its migration path and to measure its lifetime, assigning a certain criterion for the cluster breakup. In addition, the data obtained from the WS analysis coupled with the corresponding positions of He atoms allows to determine the occupation of WS cells by He atoms and thus allows to characterize the evolution of the structure of the He-V clusters during the MD run. For example, the transformation of the He₄V₁ cluster into He₄V₂ with the corresponding emission of a self-interstitial atom could easily be detected based on numerical criteria.

MS calculations have shown that helium atoms and vacancies are bound to each other up to the fifth nearest neighbor distance, hence the cluster dissociation is assumed to occur when at least one vacancy or He atom is found at a distance larger than $\sqrt{3}a_0$ from any other vacancy/He atom that belongs to the cluster. When a He-V cluster was registered to break apart by emitting a He (since mainly He-rich clusters were studied), the detached He atom executed fast 3D motion and rejoined the cluster within a short period of time, being incapable of escaping due to the imposed periodic boundary conditions. By performing a relatively long

MD run, it was possible to accumulate a sufficient number of dissociation events (from tens up to a few hundreds) and obtain a reliable value for the cluster lifetime. Similarly, the duration of a MD run was controlled to obtain a meaningful number of cluster migration jumps for an accurate estimate of the diffusion coefficient. A typical length of the performed MD runs was about 50–100 ns.

The diffusion coefficient of a He-V cluster, $D_{\text{He-V}}(T)$, can be obtained from atomistic simulations using the well-known Einstein equation (see, e.g., Ref. 33),

$$D_{\text{He-V}}(T) = \frac{\overline{R^2}(T)}{2nt_{\text{sim}}}, \quad (3)$$

where $\overline{R^2}$ is the mean square displacement of a migrating defect and is a function of temperature, n is the dimensionality of the motion (3 in the present case), and t_{sim} is the simulation time. After repeating the calculation for different temperatures, the $D_{\text{He-V}}(T)$ curve can be produced by fitting the different points to the Arrhenius expression,

$$D_{\text{He-V}}(T) = D_{0,\text{He-V}} e^{-E_m^{\text{He-V}}/k_B T}. \quad (4)$$

Here k_B is Boltzmann's constant, while the migration energy $E_m^{\text{He-V}}$ and the prefactor $D_{0,\text{He-V}}$ are the free parameters of the fit, whose values are obtained from the regression on the collected points. Similar treatment applied to the cluster lifetime $\tau_{\text{He-V}}(T)$, i.e., the period of time required to emit a He atom, can be used to estimate the dissociation energy E_d and an attempt frequency prefactor ν_0 as

$$\tau_{\text{He-V}}(T) = \nu_{0,\text{He-V}}^{-1} e^{E_d^{\text{He-V}}/k_B T}. \quad (5)$$

III. RESULTS

A. Binding and dissociation energy of He-V clusters

The dependence of the binding energy of He_{*n*}V_{*m*} clusters (with n and m varied from 0 to 4) on the He/V ratio estimated in the pure Fe and Fe–10Cr alloy is presented in Figs. 2(a) and 2(b), respectively. As has been shown by previous MS (Ref. 11) and DFT (Ref. 17) calculations, the binding energy mainly depends on the He/V ratio, and much less on the cluster size. One can also mention that the effect of Cr on

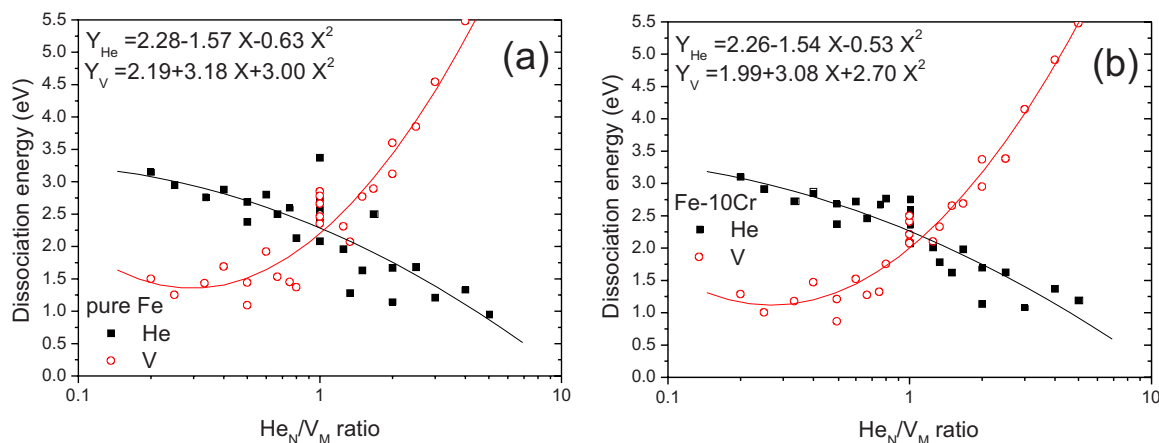


FIG. 3. (Color online) The dissociation energy of He-V clusters vs He/V ratio estimated using MS techniques in the pure Fe and Fe–10Cr alloy.

the absolute value of the binding energy and on the corresponding crossover of the two curves is insignificant.

Estimation of the dissociation energy of He-V clusters in the alloy requires knowledge of the migration energy of a vacancy and He interstitial. These were obtained by calculating the slope of Arrhenius plot of the diffusion coefficient of the species in the alloy. The corresponding migration energies were calculated to be 0.51 and 0.077 eV for a vacancy and He, respectively. While $E_m(\text{He})$ is unchanged by alloying of Fe, the migration energy of a vacancy is lower by 0.1 eV in the alloy as compared to pure Fe.

Combining the data on the binding energy of He-V clusters and migration energy of a He and vacancy, the dissociation energy curves were obtained for pure Fe and Fe–10Cr, shown in Figs. 3(a) and 3(b), respectively. As can be seen from Fig. 3, the clusters with He/V ratio close to 1–1.5 are the most stable ones in both materials. We thus see that the presence of 10% of randomly distributed Cr atoms essentially does not affect the absolute value of the dissociation energy nor the He density in the most stable He-V clusters. In addition, note that the He/V ratio corresponding to the crossover between the He and vacancy dissociation curves (located at ~ 1.1) and the corresponding dissociation energy (~ 2.4 eV) are in much better agreement with the DFT data reported in Ref. 17, than the data obtained with the earlier developed interatomic potentials for Fe–He system, which suggest an optimum He/V ratio of ~ 1.8 and the corresponding $E_d \sim 3$ eV.¹¹

The relaxed configurations of the He_N and He_NV_1 clusters whose stability and mobility was studied here by MD are presented in Fig. 4. The structures of pure He clusters, that are shown in Figs. 4(a)–4(c), are well in line with those obtained by DFT in Ref. 15, i.e., He atoms prefer to occupy closest interstitial sites, thus maximizing the number of He–He nearest neighbors and, respectively, minimizing the number of He near to Fe. In the case of the He_NV_1 clusters, shown in Figs. 4(d)–4(f), He atoms were found to occupy the WS cell space of the removed metallic atom and to form symmetrical clusters. In particular, He_2V_1 was observed to relax into $\langle 110 \rangle$ dumbbell configuration, He_3V_1 represents a triangular configuration laying in a $\{100\}$ plane. Adding one more He atom to He_3V_1 results in the formation of the tet-

rahedral configuration made of four He atoms, where the pairs of He atoms are connected by $\langle 100 \rangle$ and $\langle 010 \rangle$ vectors, as shown in Fig. 4(f).

B. Mobility of He-V clusters

1. Mobility of pure He clusters

Among the clusters studied here, the pure He clusters were found to exhibit the fastest motion. Due to the binding energy not exceeding 0.6 eV, their mobility was mainly studied in the low temperature range between 100 and 500 K. At 500 K, the lifetime of the most stable He_4 cluster did not exceed a few nanoseconds, even within this relatively short period of time the cluster was seen to cover a significant distance (of about a few tens of nanometers) before emitting a He atom. Using the methodology described in Sec. II, the diffusion coefficients of He clusters were estimated in Fe and Fe–10Cr and the results are plotted in Fig. 5. The corresponding migration energies and prefactors for diffusion coefficients are presented in Fig. 6, estimated by fitting the MD results to Eq. (4).

The motion of He clusters occurred via migration of He atoms performing individual jumps into neighboring interstitial positions. It was, however, impossible to distinguish between the tetra- or octahedral interstitial position of jumping He atoms due to thermal vibrations. The trajectory that the He clusters passed was clearly 3D. The obtained migration energies for He clusters are of the order of the migration energy of a He interstitial, i.e., ~ 0.07 eV. Therefore, the fact that the He atoms bound in a cluster do not strictly occupy

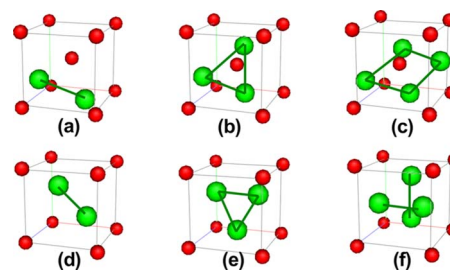


FIG. 4. (Color online) Configurations of relaxed He_N [(a)–(c)] and He_NV_1 [(d)–(f)] clusters in pure Fe.

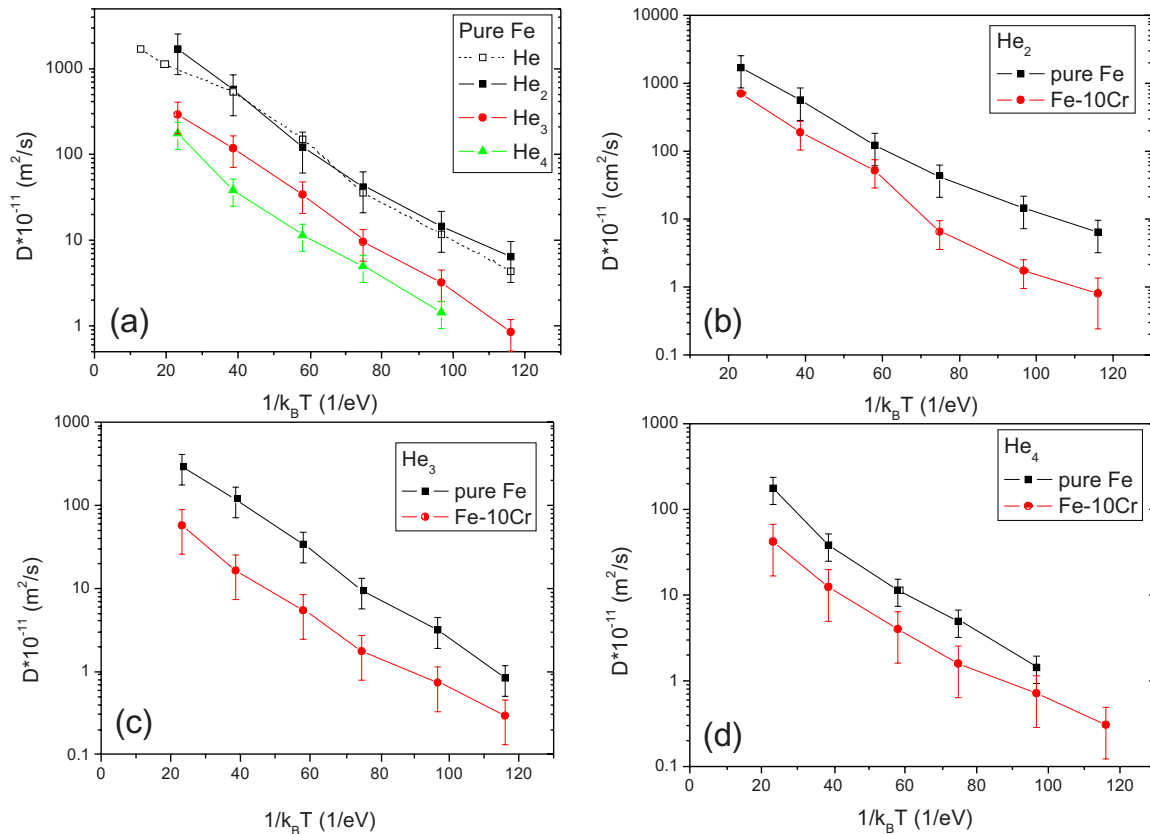


FIG. 5. (Color online) Diffusion coefficients of pure He clusters together with standard errors as a function of temperature.

tetrahedral positions does not significantly affect their migration energy. In turn, the effective migration energy of He clusters is even slightly lower than $E_m(\text{He})$, as can be seen from Fig. 6. However, the overall diffusion coefficient of He clusters decreases with cluster size, as shown in Fig. 5(a). The corresponding reduction in the diffusivity is expressed in the decrease in the diffusion coefficient prefactor, see Fig. 6(b).

The mechanism of motion of pure He clusters was seen to be identical in Fe and Fe–10Cr alloys. Yet, the presence of 10% Cr in the Fe matrix causes a reduction in the mobility of the He clusters, which is seen from the comparison of the diffusion coefficients presented in Figs. 5(b)–5(d). Indeed, the obtained migration energies for He₂ and He₃ clusters are

slightly higher than those in pure Fe [see Fig. 6(a)], while $D_0(\text{He}_4)$ is lower in the alloy. It is, however, difficult to conclude that the presence of Cr leads to the increase in the migration energy, since the associated error can reach up to 20%–30% of the migration energy value.

2. Mobility of He_nV₁ clusters

Another group of studied clusters, He_nV₁, appeared to have much lower diffusivity than the pure He clusters but yet measurable at the MD time scale. The mobility and thermal stability of these clusters were studied in the temperature range of 960–1800 K. The obtained migration energies and prefactors of diffusion coefficients are summarized in Table

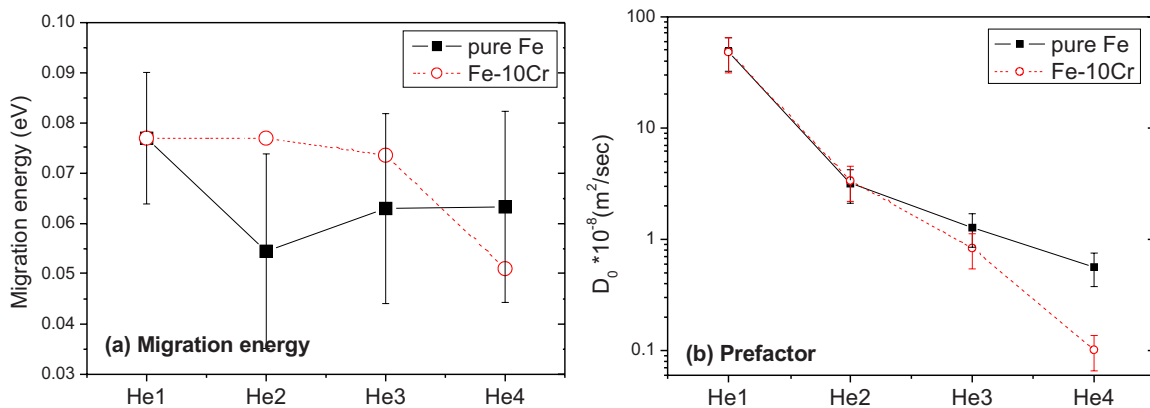


FIG. 6. (Color online) Migration energy and prefactor estimated by fitting the data on diffusion coefficients of pure He clusters. Standard errors of the mean are also shown.

TABLE I. The parameters of diffusivity of some He-V clusters estimated from MD simulations in pure Fe. The standard errors of the mean of a migration energy are given as well.

	He ₂ V ₁	He ₃ V ₁	He ₄ V ₁	He ₂ V ₃
Pure Fe				
E_m (eV)	0.33 ± 0.06	0.31 ± 0.04	0.28 ± 0.06	0.55 ± 0.09
D_0 (m ² /s)	1.16×10^{-7}	2.00×10^{-8}	3.68×10^{-9}	7.82×10^{-9}
Fe-10Cr				
E_m (eV)	0.31 ± 0.07	0.30 ± 0.05	0.31 ± 0.07	0.53 ± 0.12
D_0 (m ² /s)	3.34×10^{-7}	3.20×10^{-8}	2.13×10^{-9}	9.93×10^{-9}

I. As can be seen, the migration energies of He₂V₁, He₃V₁, and He₄V₁ clusters are essentially higher than those of the pure He clusters, but at the same time, they are a factor of 2 lower than the migration energy of a single vacancy in pure Fe (0.65 eV).

Application of visualization tools and postprocessing analysis of the data on the crystal defects allowed to identify the mechanism of motion of these clusters. Initially all He atoms were occupying a space provided by the metallic vacant site. Then, one of the neighboring Fe atoms was pushed away from its site to the interstitial position, so that the He_{*n*}V₁ (*n*=2, 3, 4) cluster could spread over two atomic volumes. Its center of mass was located somewhere around $\frac{1}{4}, \frac{1}{4}, \frac{1}{4}$ position in the bcc lattice. After that, a Fe self-interstitial atom, being attracted to the cluster, jumps back in one of the two available lattice sites (i.e., WS volume assign to a lattice site). The He_{*n*}V₁ clusters were also seen to execute a 3D migration path. The estimated migration energies are of the order of 0.3 eV, suggesting that the motion mechanism is governed by the transformation of the He_{*n*}V₁ cluster into He_{*n*}V₊₁-SIA complex or migration of a SIA, needed for the displacement of a He-V cluster center mass. From the point of view of the energy balance, the above mentioned transformation requires 0.45, 0.49, and 0.86 eV for He₄V₁, He₃V₁, and He₂V₁, respectively. The migration energy of a SIA in the <110> dumbbell configuration in Fe is 0.31 eV,²⁵ which is only slightly higher than the value of $E_m(\text{He}_n\text{V}_1)$ estimated here. Taking into account, that $E_m(\text{He}_n\text{V}_1)$ were found to be only weakly dependent on the cluster size, it seems reasonable to assign the controlling mechanism to the SIA migration.

3. Mobility of He₂V₃ cluster

The He₂V₃ cluster was observed to execute a ring diffusion mechanism, which implies the motion of two He atoms located in the substitutional positions via exchange with the available vacancy site. Thus, the cluster was seen to move as a whole by consecutive He-vacancy and Fe-vacancy exchanges, and the two He atoms could stay apart as far as fourth nearest neighbor. This mechanism is very similar to the motion of a Cu₂-vacancy cluster in Fe.³⁴ The mobility of this cluster is therefore governed by the vacancy diffusion and the cluster exhibits a 3D path. The estimated migration energy, found to be slightly lower than that of a single vacancy in pure Fe, suggests that the local lattice strain due to the presence of substitutional He atoms near a vacancy affects its migration energy. Finally, it should be mentioned that the mobility of this cluster has been studied using lattice KMC in Ref. 18, where the diffusion coefficient was estimated at 573 K to be 1.6×10^4 nm²/s. Using the values provided in Table I, one can find that at the same temperature $D(\text{He}_2\text{V}_3)$ is equal to 9.92×10^4 nm²/s, which is at least the same order of magnitude. This is very reasonable agreement taking into account a number of simplifications behind the LKMC technique.

C. Lifetime of He-V clusters

The He-V clusters which were observed to dissociate within the time span of the MD run and whose lifetime could be reliably measured are listed in Table II. These were only the clusters with high He/V ratio or pure He clusters, seen to dissociate by emitting He atoms. The corresponding dissociation energies and attempt frequency prefactors were estimated by fitting Eq. (5) to the data set on the lifetime of the clusters. The obtained results are summarized in Table II and are compared with the dissociation energies obtained from MS calculations in Fe. The MS data for Fe-10Cr alloys are not included in Table II, since they are essentially the same as for pure Fe (see Sec. III A).

In general, the MD-obtained dissociation energies are in reasonable agreement with the corresponding values estimated using MS calculations. The largest discrepancy occurs in the case of the He₄V₂ cluster, where the difference in the dissociation energies obtained by the two methods is 0.6 eV. The dissociation energies obtained from MD for pure He

TABLE II. Parameters of lifetime of some He-V clusters estimated from MD simulations in pure Fe and Fe-10Cr alloys and dissociation energy of a He from He-V clusters estimated in pure Fe using MS simulations. The standard errors of the mean of a migration energy are given as well.

Type of cluster	Pure Fe, MD results		Fe-10Cr alloy, MD results		MS results
	$\nu_0(s^{-1}) \times 10^{13}$	E_d (eV)	$\nu_0(s^{-1}) \times 10^{13}$	E_d (eV)	E_d (eV)
He ₂	0.245	0.14 ± 0.03	0.969	0.18 ± 0.05	0.2
He ₃	16.9	0.35 ± 0.12	8.00	0.32 ± 0.04	0.4
He ₄	40.0	0.59 ± 0.20	12.0	0.61 ± 0.10	0.71
He ₂ V ₁	19.6	1.15 ± 0.31	23.1	1.17 ± 0.31	1.14
He ₃ V ₁	187	1.40 ± 0.32	591	1.39 ± 0.28	1.21
He ₄ V ₁	18.8	1.15 ± 0.20	19.5	1.03 ± 0.13	1.32
He ₄ V ₂	7.00	1.35 ± 0.24	5.97	1.04 ± 0.34	1.67

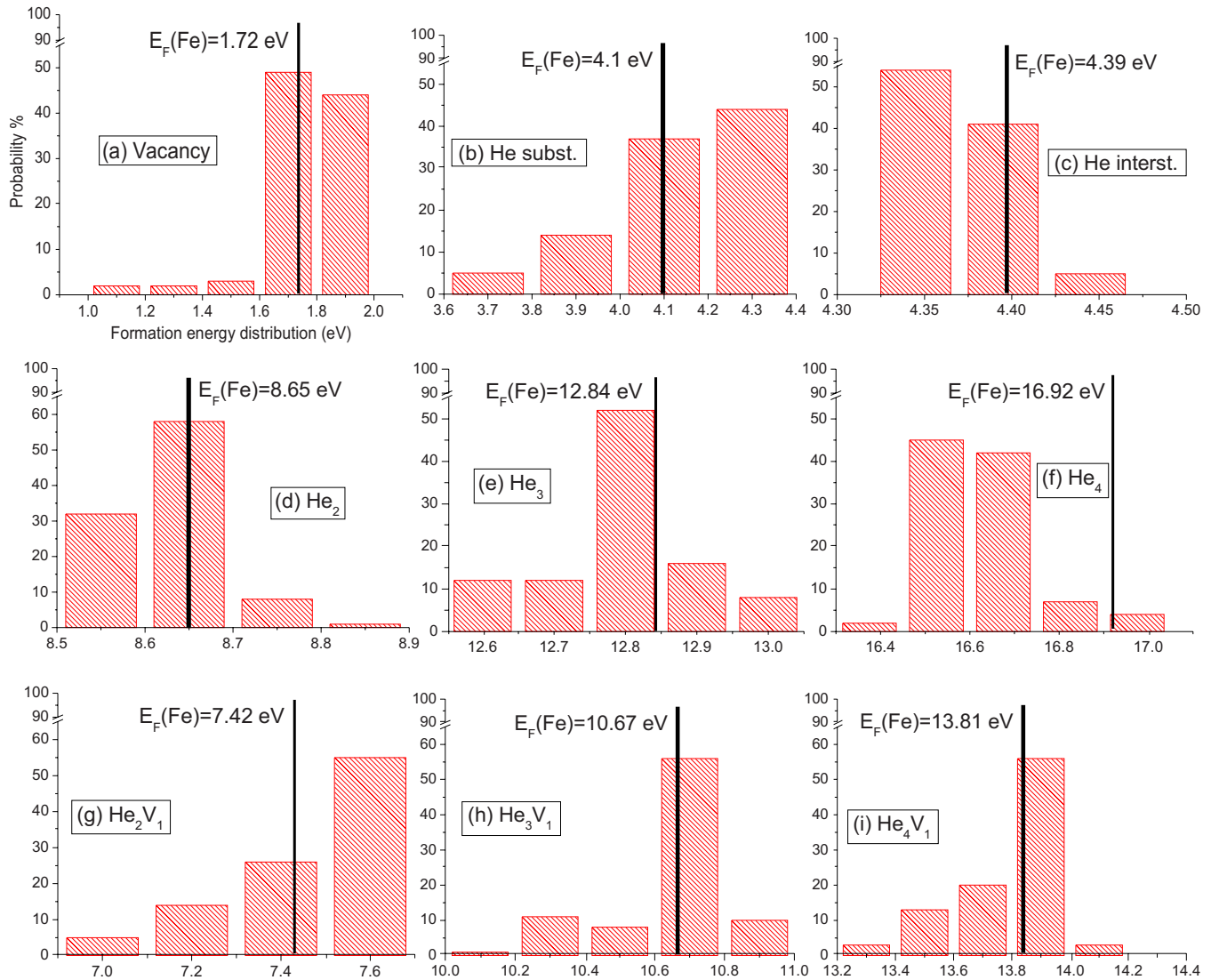


FIG. 7. (Color online) The formation energy probability distribution $P(E_F)$ as a function of the formation energy in Fe–10Cr random alloy for (a) a single vacancy, (b) He atom in a substitutional position, (c) He atom in the interstitial position (tetrahedral site), [(d)–(f)] clusters of He interstitials and [(g)–(i)] some He–V clusters, as specified in the corresponding figures. The black bar denotes the formation energy of a given defect in pure Fe.

clusters are only slightly less than the predictions of MS calculations. It should, however, be stressed that the obtained attempt frequencies of some clusters are much higher than the Debye frequency ($6 \times 10^{12} \text{ s}^{-1}$). In particular, ν_0 of some large He–V clusters (e.g., He_3V_1) appears to be as high as 10^{15} s^{-1} . The very high attempt frequency for the dissociation might be attributed to the large discrepancy between masses of He and metallic atoms, so that vibration modes of He atoms bound in a cluster are different from those of surrounding metallic atoms. Note that the usual practice of Monte Carlo simulations is to describe the rate of dissociation or migration events taking Debye frequency as the attempt frequency (e.g., Refs. 18–20). The observed discrepancy clearly suggests that the real lifetime of some He-rich clusters could be much shorter than by relying on the estimations coming from MS results.

D. Effect of Cr on the mobility and lifetime

Summarizing the obtained results on the mobility and thermal stability of the studied He–V clusters, one may con-

clude that there is no drastic effect of the presence of 10% of Cr on the cluster properties. In particular, the dissociation energy and attempt frequency for He–V clusters estimated from both MD and MS simulations are practically the same in Fe and Fe–10Cr alloys.

The only essential effect of Cr appeared in the case of pure He clusters, whose diffusivity was reduced in Fe–10Cr as compared to Fe. The observed reduction is most likely related to the trapping of He clusters, being bounded to some specific Cr clusters. The distributions of the formation energy probability of He clusters presented in Appendix B [see Figs. 7(d)–7(f)] reveals a presence of states for the He cluster (with a non-negligible probability), that exhibit essentially lower formation energy than the average value, given in Table VII. For example, $E_F(\text{He}_3)$ and $E_F(\text{He}_4)$ in Fe–10Cr are 12.8 and 16.5 eV, whereas the formation energy of these clusters may be as low as 12.6 and 16.4 eV, i.e., reduced by 0.1–0.2 eV in some configurations. This reduction in the cluster formation energy is significant compared to the effective migration energy estimated from MD simulations, which

is the order of 0.05 eV. The He clusters, while migrating through the lattice, would encounter these low energy configurations. The time required for the cluster to escape from such a configuration should be proportional to $\exp(E_b + E_m)/k_B T$, where E_b is the binding energy of the cluster to the surrounding Cr atoms. This is why some particular Cr configurations, that result in the essential decrease in the formation energy of the He or He-V clusters, might act as traps, whose presence in the matrix decreases the mobility of the clusters.

IV. CONCLUDING REMARKS

Summarizing, we have performed atomistic simulations in both static (MS) and dynamic (MD) conditions in order to characterize properties of small He-V clusters in bcc Fe and Fe-10Cr alloys. MS calculations were used to obtain the values of the dissociation energy as a function of He density in the clusters. The results obtained in pure Fe have shown much closer agreement with existing DFT data on the optimum He-to-vacancy ratio and the corresponding dissociation energy (~ 2.4 at He/V ~ 1) than previously existing potentials did,¹¹ as discussed in Sec. III A. No significant effect of alloying of Fe by 10% of Cr on the dissociation energy diagram was found.

MD simulations were used to characterize the mechanisms of motion and to estimate the parameters of diffusivity and thermal stability of pure He and He-rich clusters. One of the important findings of this work is that small pure He clusters were seen to move as fast as He interstitials. Taking into account that the estimated migration energy of these clusters is extremely small, one may definitely conclude that such objects would cover a substantial distance during their lifetime. In addition, it has been shown that the mobility of the pure He clusters is retarded in Fe-10Cr alloys, which was tentatively associated to the “configuration” trapping originating from the presence of low energy states for the He clusters due to some specific Cr arrangements significantly decreasing their formation energy (see Sec. III B).

Modeling He-V clusters, two different mechanisms of motion were observed for the He-rich (He_nV_1) and vacancy-rich (He_2V_3) clusters. The first mechanism involves formation of a metallic interstitial atom, whose motion causes the displacement of the He-V cluster. The corresponding migration energy was estimated to be ~ 0.3 eV. On the other hand, the diffusivity of He_2V_3 cluster was controlled by the mobility of a vacancy, with the migration energy of 0.55 eV. Characterization of the thermal stability of the clusters was also performed based on the results of MD simulations. In most of the cases, the estimated dissociation energies from MD were in line with the corresponding data obtained from MS calculations. It is important to note that the dissociation attempt frequencies for some of the studied clusters were found to be two orders of magnitude higher than the Debye frequency. Thus, usage of the Debye frequency of Fe, usually taken as $(6-10) \times 10^{12} \text{ s}^{-1}$, to estimate the rate of dissociation events of He-V clusters might be an oversimplification.

Finally, we note that recent KMC studies addressing kinetics of He desorption under He-implantation conditions

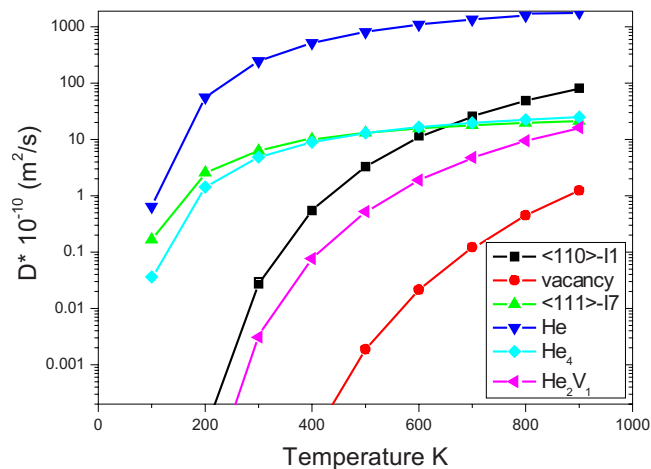


FIG. 8. (Color online) Diffusion coefficient of different types of defects in pure Fe, namely, self-interstitial atom in the $\langle 110 \rangle$ dumbbell configuration (Ref. 35), a single vacancy, one dimensional migrating 7-SIA cluster in the $\langle 111 \rangle$ configuration (Ref. 38), an interstitial He atom, the He_4 and He_2V_1 cluster.

have shown that introduction of the mobility of self-interstitial atoms plays an important role.¹⁹ In particular, by accounting for the mobility of not only single self-interstitial atoms but also their clusters, a delay in the He release was observed. In the mentioned study, however, no mechanisms allowing for the mobility of pure He and He-rich vacancy clusters were introduced and the clusters were simply assumed to be immobile. Such simplification is justified if the objects, assumed to be immobile, are moving drastically slower than the other migrating species presenting in the system, i.e., point defects, their clusters, and He interstitials.

The results of this work suggest that this assumption is not well justified. The comparison of the diffusion coefficients of the $\langle 110 \rangle$ self-interstitial atom,³⁵ $\langle 111 \rangle$ self-interstitial atom cluster containing seven defects,³⁵ a single vacancy, He interstitial, He_4 and He_2V_1 clusters is presented in Fig. 8. All results shown in the figure were obtained using the currently employed IAP (Table III). Clearly, the mobility of pure He and He_2V_1 clusters is higher than that of a vacancy and comparable with that of a single self-interstitial atom. As soon as interstitials and their clusters become mobile, a part of them would recombine with vacancies in the already formed He-V clusters, which should lead to the formation of He-V clusters enriched by He (i.e., with high He/V

TABLE III. Formation energies of helium interstitials in iron and in chromium for substitutional, octahedral, and tetrahedral positions. All values are in eV.

Fe-He		Subs.	Octa.	Tetr.
DFT	Seletskaiia ^a	4.08	4.60	4.37
	Fu ^b	4.22	4.57	4.39
MD	This work	4.10	4.51	4.39
Cr-He				
DFT	This work	5.00	5.37	5.20
MD	This work	5.01	5.34	5.25

^aReferences 12 and 13.

^bReference 17.

ratio). The appearance of a substantial amount of He-rich clusters, moving faster than vacancy-rich clusters, should result in an additional He release naturally absent in the KMC simulations performed in Ref. 19. It is therefore of interest to check if the introduction of the migration mechanisms for He-V clusters enriched by He leads to a better agreement with experimental data. The proposed simulations would also probably resolve the necessity for the introduction of traps for SIA clusters, whose origin is so far not fully understood.¹⁹ Moreover, the value of the trapping energy of 1.0 eV and concentration (1–10 ppm) is not justified, as discussed in Ref. 19.

V. CONCLUSIONS

Based on the results obtained using MS and MD techniques coupled with a recently developed set of IAPs for Fe–Cr–He system we may draw the following conclusions.

- (i) The dissociation energies of small He-V clusters are not significantly affected by the presence of 10% Cr in Fe matrix as compared to pure Fe.
- (ii) The effective migration energy of He interstitial is not affected by the presence of Cr.
- (iii) Small pure He clusters with size up to four atoms exhibit fast 3D motion, with a migration energy of about 0.05 eV.
- (iv) The presence of Cr in the matrix retards the mobility of pure He clusters, it does not, however, significantly change their migration energy.
- (v) The dissociation energy of He-V clusters estimated from MD simulations was found to be in good agreement with the values obtained from static simulations. The prefactor of the dissociation jump frequency, however, was seen to be much higher than the Debye frequency.

ACKNOWLEDGMENTS

This work was performed in the framework of the 7th Framework Programme collaborative project GETMAT, partially supported by the European Commission, grant Agreement No. 212175. Calculations were performed at Fermi computer cluster in SCK-CEN (Belgium) and the Ametisti at the University of Helsinki (Finland).

APPENDIX A: POTENTIALS FOR FE-HE AND CR-HE

As mentioned in Sec. I, we need potentials for Fe–He and Cr–He that work well with the existing Fe potential by Ackland²⁶ and Cr potential by Olsson.²¹ For Fe–He, a recently developed potential with three-body terms,¹³ further developed in Ref. 36, produces interstitial properties in good agreement with DFT data, which the potential from the 1960s by Wilson³⁷ failed to do.¹⁷ We have developed a Fe–He potential based on a pair potential formalism, which also proved to be enough to describe interstitial He in Fe in accordance with DFT data.³⁸ Cr–He has not been studied much in the literature, and we set out to calculate the needed

TABLE IV. Parameters for the Fe–He and Cr–He potentials.

	Fe–He	Cr–He
a (eV)	26.65	0.6115
b (eVÅ)	–15.0	18.87
c (1/Å)	1.856	1.454
r_1 (Å)	1.0	1.0
r_2 (Å)	1.2	1.22
r_c (Å)	3.7	3.75
r_d (Å)	0.25	0.1
p_3 (eV/Å ³)	62.020 897	27.154 909
p_2 (eV/Å ²)	–96.287 579	14.777 250
p_1 (eV/Å)	–38.548 739	–163.425 31
p_0 (eV)	79.266 283	130.802 57

DFT data and develop a potential. Here the Cr–He potential is presented, along with the parameters for the Fe–He potential.

1. DATA

We have performed *ab initio* calculations using the DMO197 program package^{39,40} to get interaction energy versus distance data for the Fe–He and Cr–He dimers. The standard DMOL orbitals were augmented with hydrogenic orbitals.⁴¹ This approach has previously been shown to give interaction energies in the repulsive region which are in line with a fully numerical Hartree–Fock–Slater (X_α) method.^{42,43} The obtained dimer energies, listed in Tables IV and V were used to fit the potentials for short-range interaction. The dimer potentials are, however, not adequate for correct description of helium defects in the metals.

Properties of He defects in Fe were characterized using DFT calculations performed by Seletskaja *et al.*^{13,36} and by Fu and Willaime¹⁷ with VASP and SIESTA DFT codes, respectively. The necessary He defect properties in Cr have been calculated using the VASP code to obtain a data set for the fitting of the Cr–He potential. The obtained formation energies of different He configurations in Cr are listed in Table VI and the migration energy landscapes are given in Figs. 9 and 10.

Details of the performed DFT calculations can be summarized as follows. Each defect configuration was relaxed in a supercell containing 128 bcc lattice points. Spin polarization was included with the initial spin-order antiferromagnetic for Cr. The exchange-correlation was treated in the generalized gradient approximation.^{44,45} The presence of He requires a relatively high cutoff energy in the plane-wave expansion, so the PAW pseudopotentials^{46,47} were applied with a cutoff energy of 478 eV. The relaxation was performed at constant volume set to the equilibrium bulk volume of pure Cr. The Brillouin zone was sampled in a $3 \times 3 \times 3$ -grid using the Monkhorst and Pack scheme.

2. POTENTIAL CONSTRUCTION

Considering the repulsive nature of helium in iron and chromium, and the simplified picture of positive nuclei in an electron cloud, a natural function form to choose is a

TABLE V. Data listed for the Fe–He DMol dimer potential.

r (Å)	f (eV)	r (Å)	f (eV)	r (Å)	f (eV)
0.001	742 308.990 941	0.100	3900.770 613	0.560	83.527 946
0.002	367 929.108 134	0.120	2932.205 400	0.580	74.561 277
0.003	243 146.799 839	0.140	2279.876 865	0.600	66.673 635
0.004	180 789.363 700	0.160	1814.874 546	0.620	59.702 486
0.005	143 386.113 350	0.180	1468.779 606	0.640	53.513 466
0.006	118 462.568 194	0.200	1202.690 203	0.660	47.995 909
0.007	100 673.425 256	0.220	993.428 081	0.680	43.060 309
0.008	87 344.768 144	0.240	826.385 481	0.700	38.631 227
0.009	76 990.273 923	0.260	691.670 110	0.720	34.647 305
0.010	68 719.745 430	0.280	582.160 568	0.740	31.055 904
0.011	61 963.988 467	0.300	492.614 357	0.760	27.814 882
0.012	56 344.366 351	0.320	418.974 166	0.780	24.886 748
0.013	51 597.954 831	0.340	358.075 144	0.800	22.238 914
0.014	47 536.487 083	0.360	307.477 324	0.820	19.843 742
0.015	44 022.879 513	0.380	265.243 036	0.840	17.678 637
0.016	40 954.622 254	0.400	229.812 713	0.860	15.721 379
0.017	38 252.408 019	0.420	199.952 152	0.880	13.953 087
0.018	35 855.089 452	0.440	174.682 721	0.900	12.355 634
0.019	33 714.656 575	0.460	153.202 236	0.920	10.914 554
0.020	31 792.090 048	0.480	134.857 477	0.940	9.615 746
0.040	13 861.000 825	0.500	119.113 258	0.960	8.446 703
0.060	8 159.846 377	0.520	105.536 708	0.980	7.395 154
0.080	5 445.595 238	0.540	93.772 294	1.000	6.450 862

screened Coulomb potential. The function form $f(r)=(a+b/r)\exp(-cr)$ was found to be suitable for a satisfactory reproduction of He defects in the metals. The terms a and b/r give a better possibility to affect short- and long-range parts of the potential. Adding other terms and parameters would give more flexibility in the fitting, but with the limited data set to fit, it would not guarantee transferability of the potentials.

To obtain a smooth transition between the dimer potential and the above introduced functional term, we used a polynomial spline satisfying the energy and its first derivative at the connection nodes. The function form of the spline is

$$f(r_{ij}) = \begin{cases} \text{DMOL-potential}, & r_{ij} \leq r_1 \\ p_3 r_{ij}^3 + p_2 r_{ij}^2 + p_1 r_{ij} + p_0, & r_1 \leq r_{ij} \leq r_2 \\ \left(a + \frac{b}{r_{ij}}\right) e^{-cr_{ij}} f_c(r_{ij}), & r_{ij} \geq r_2, \end{cases} \quad (\text{A1})$$

where the cutoff function f_c is given by

$$f_c(r_{ij}) = \begin{cases} 1, & r_{ij} \leq r_c - r_d, \\ \frac{1}{2} \left(1 - \sin \frac{\pi(r_{ij} - r_c)}{2r_d}\right), & |r_c - r_{ij}| \leq r_d, \\ 0, & r_{ij} \geq r_c + r_d, \end{cases} \quad (\text{A2})$$

TABLE VI. Data listed for the Cr–He DMol dimer potential.

r (Å)	f (eV)	r (Å)	f (eV)	r (Å)	f (eV)
0.002	339 782.473 128	0.080	5087.948 470	0.450	167.88 225
0.004	167 031.551 471	0.100	3651.512 223	0.500	123.499 933
0.006	109 501.603 048	0.120	2750.904 432	0.550	92.762 362
0.008	80 769.484 343	0.140	2146.655 359	0.600	70.895 227
0.010	63 566.354 974	0.160	1717.571 854	0.650	54.886 597
0.012	52 135.961 143	0.180	1398.887 168	0.700	42.836 359
0.014	44 000.416 731	0.200	1153.836 523	0.750	33.548 373
0.016	37 919.218 234	0.240	805.173 398	0.800	26.260 331
0.018	33 208.159 719	0.280	575.229 695	0.850	20.481 583
0.020	29 454.455 425	0.320	418.770 824	0.900	15.880 285
0.040	12 880.717 942	0.360	310.252 422	0.950	12.216 320
0.060	7 606.147 481	0.400	233.786 173	1.000	9.309 422

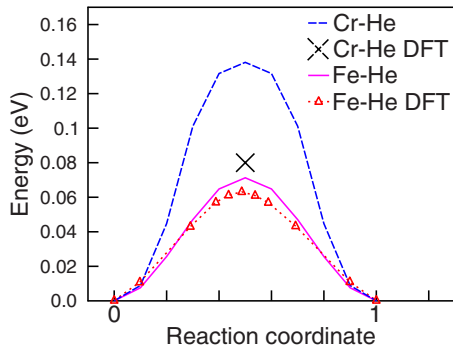


FIG. 9. (Color online) The migration barrier for the migration of helium in iron from one tetrahedral interstitial position to a neighboring tetrahedral position.

which is a function that goes smoothly from one at $r_{ij} \leq r_c - r_d$ to zero at $r_{ij} \geq r_c + r_d$. This cutoff function is a standard type used in Tersoff-type potentials.⁴⁸ The spline nodes and parameters for the cutoff function were deduced based on the neighborhood around the helium atom for the defect structures of interest.

The potentials were fitted to the formation energy of the substitutional He and interstitial He in the tetrahedral and octahedral configurations in iron and chromium. After calculating the migration barriers (see Sec. A 3) the parameters were refitted by adjusting the weights of the fitted properties, so that a set of parameters that satisfactory reproduce both the formation energies and migration barriers was obtained.

The comparison of the fitted values versus DFT data is presented in Table VI. It can be seen that the departure of the fitted formation energies from the original DFT results is within 1%–2%.

3. RESULTS

The comparison of the migration barriers calculated using the derived potentials with the DFT data from Ref. 17 for Fe–He and from this work for Cr–He is presented in Fig. 9. The barriers were computed using the drag method as was done in the corresponding DFT work.¹⁷ The migration barrier of the interstitial He (in tetrahedral position) in Fe obtained with the potential (0.07 eV) agrees very well with the DFT value (0.06 eV). In Cr, the barrier was found to be overestimated by the potential (0.14 eV) in comparison with the DFT estimated barrier (0.08 eV). The characterization of

the motion of a substitutional He atom requires consideration of the mobility of the HeV₂ complex as pointed out by Fu and Willaime.¹⁷ The energy landscape for this defect is shown in Fig. 10. Both potentials reproduce parts of the energy landscapes well compared to the DFT data, while some features are in rather poor agreement. The Fe–He potential is discussed in greater detail in Ref. 38.

Considering the migration barrier landscape in Cr, we can see that the height of the barrier at (d) is very well reproduced, about 1.4 eV with the potential and 1.5 eV with DFT. According to the DFT results, however, the configuration (e) is energetically more favorable than configuration (c), which is not reproduced by the fitted potential. Given the height of the migration barriers in the HeV₂ complex, the migration properties can still be expected to be reasonable with the derived potential.

APPENDIX B: FORMATION ENERGY OF HE, VACANCY, AND HE-V CLUSTERS IN FE-10CR ALLOY

The formation energy of a defect in a concentrated random alloy depends on the particular local atomic arrangement of solutes around a defect, as has been recently shown in Ref. 25 for the case of a self-interstitial atom in Fe–Cr alloys. The average formation energy can be estimated by calculating the formation energy of the same defect but varying local atomic arrangement, which should correspond to an alloy of a given concentration and distribution of solute atoms. The easiest way to perform such calculations for the random alloy is to insert a defect in all possible sites of a MD box, containing a given concentration of randomly distributed solutes, as was done in this work.

Before the insertion of a vacancy and/or He atom, the perfect crystallite was relaxed at the corresponding equilibrium lattice constant, which depends on C_{Cr} , and its cohesive energy $E_{ref}(C_{Cr})$ has been recorded. After a He–V complex was created, the system was relaxed down to zero temperature keeping the volume constant and without applying any constraint to the atoms. The static relaxation was performed using quench procedure³⁰ to achieve the convergence of 10^{-10} eV/atom in the crystal cohesive energy. The formation energy was then defined as¹³

$$E_f = E_{N(Fe+Cr),M(He)} - N \cdot E_{Fe-10Cr} - M \cdot E_{He}. \quad (B1)$$

Here, $E_{Fe-10Cr}$ is the cohesive energy (per atom) of a perfect Fe–10Cr crystal before a defect was inserted; $E_{N(Fe+Cr),MHe}$ is the total energy of the relaxed Fe–10Cr crys-

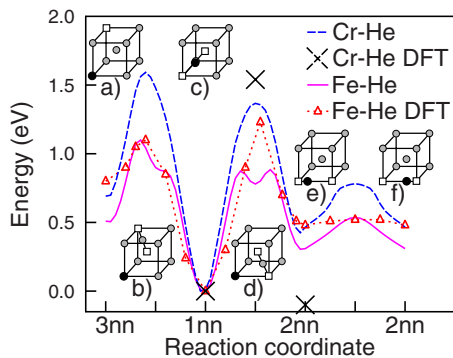


FIG. 10. (Color online) The energy landscape for HeV₂ in Fe and in Cr.

TABLE VII. The average formation energies of He–V clusters obtained by static calculations in Fe–10Cr random alloy. All values are given in eV.

He	Vac					
	0	1	2	3	4	5
0	...	1.76	3.36	4.71	6.07	7.13
1	4.37	4.13	5.43	6.43	7.6	8.48
2	8.63	7.43	7.51	8.41	9.37	10.07
3	12.79	10.81	10.33	10.29	11.14	11.79
4	16.62	13.88	13.11	12.95	13.05	13.46
5	20.44	17.13	15.92	15.41	15.48	15.15

TABLE VIII. The average formation energies of He-V clusters obtained by static calculations in pure Fe. All values are given in eV.

He ↓ Vac →	0	1	2	3	4	5
0	...	1.72	3.3	4.62	5.93	6.99
1	4.39	4.1	5.38	6.32	7.44	8.31
2	8.65	7.42	7.44	8.28	9.21	9.89
3	12.84	10.67	10.27	10.18	11.1	11.55
4	16.92	13.81	13.06	13.36	12.88	13.88
5	20.68	17.32	15.84	15.32	15.38	14.97

tal containing N metallic atoms and M He atoms with a He-V cluster introduced; E_{He} is the total energy of an isolated He atom (taken to be zero since the classical potentials used here have no self-attraction). From the set of calculations for a given C_{Cr} , the average formation energy can be estimated straightforwardly and the corresponding formation energy probability distribution $P(E_f)$ can be built as

$$P(E_f) = \frac{n(E_f \pm \Delta E)}{n_{\text{states}}}, \quad (\text{B2})$$

where the numerator is the number of states with energy E_f within an interval $E_f \pm \Delta E$ and n_{states} is the total number of studied states. In the present calculation ΔE was varied from 0.05 up to 0.2 eV depending on the spread of the formation energy spectrum. n_{states} was 16×10^3 , i.e., each considered cluster has been inserted in every lattice site of the simulation box with size of $20 \times 20 \times 20 a_0$, where a_0 is the lattice constant. Functions $P(E_f)$ for a single vacancy, He atom in a substitutional and interstitial position and He-V clusters estimated for the Fe–10Cr alloy are presented in Fig. 7.

Regarding the obtained distributions one can see that in most of the cases the formation energy of a defect in pure Fe is coincident with the maximum probability for this energy in Fe–10Cr alloys. The average formation energies of all here studied He-V clusters estimated in Fe–10Cr and pure Fe are summarized in Tables VII and VIII, respectively. These energies were obtained using equilibrium lattice constants for Fe and Fe–10Cr 0.28553 and 0.28597 nm, respectively.

¹R. E. Stoller, *J. Nucl. Mater.* **174**, 289 (1990).

²M. B. Lewis and K. Farrell, *Nucl. Instrum. Methods Phys. Res. B* **16**, 163 (1986).

³R. Vassen, H. Trinkaus, and P. Jung, *Phys. Rev. B* **44**, 4206 (1991).

⁴R. E. Stoller and G. R. Odette, *J. Nucl. Mater.* **131**, 118 (1985).

⁵T. Ishizaki, Q. Xu, T. Yoshiie, S. Nagata, and T. Troev, *J. Nucl. Mater.* **307–311**, 961 (2002).

⁶H. Trinkaus and B. N. Singh, *J. Nucl. Mater.* **323**, 229 (2003).

⁷D. S. Gelles, *J. Nucl. Mater.* **283–287**, 838 (2000).

⁸E. Wakai, K. Kikuchi, S. Yamamoto, T. Aruga, M. Ando, H. Tanigawa, T. Taguchi, T. Sawai, K. Oka, and S. Ohnuki, *J. Nucl. Mater.* **318**, 267 (2003).

⁹K. Farrel and T. S. Bryant, *J. Nucl. Mater.* **318**, 274 (2003).

¹⁰K. Ono, K. Arakawa, and K. Hojou, *J. Nucl. Mater.* **307–311**, 1507 (2002).

¹¹K. Morishita, R. Sugano, and B. D. Wirth, *J. Nucl. Mater.* **323**, 243 (2003).

¹²T. Seletskaiia, Y. N. Osetsky, and R. E. Stoller, *Phys. Rev. Lett.* **94**, 046403 (2005).

¹³T. Seletskaiia, Y. N. Osetsky, R. E. Stoller, and G. M. Stocks, *J. Nucl. Mater.* **351**, 109 (2006).

¹⁴L. Ventelon, B. D. Wirth, and C. Domain, *J. Nucl. Mater.* **351**, 119 (2006).

¹⁵C. C. Fu and F. Willaime, *J. Nucl. Mater.* **367**, 244 (2007).

¹⁶K. Morishita, R. Sugano, B. D. Wirth, and T. D. de la Rubia, *Nucl. Instrum. Methods Phys. Res. B* **202**, 76 (2003).

¹⁷C. C. Fu and F. Willaime, *Phys. Rev. B* **72**, 064117 (2005).

¹⁸V. A. Borodin and P. V. Vladimirov, *J. Nucl. Mater.* **362**, 161 (2007).

¹⁹M. J. Caturla and C. J. Ortiz, *J. Nucl. Mater.* **362**, 141 (2007).

²⁰C. S. Deo, M. A. Okuniewski, S. G. Srivilliputhur, S. A. Maloy, M. I. Baskes, M. R. James, and J. F. Stubbins, *J. Nucl. Mater.* **361**, 141 (2007).

²¹P. Olsson, J. Wallenius, C. Domain, K. Nordlund, and L. Malerba, *Phys. Rev. B* **72**, 214119 (2005).

²²D. Terentyev, P. Olsson, L. Malerba, and A. V. Barashev, *J. Nucl. Mater.* **362**, 167 (2007).

²³C. Björkas and K. Nordlund, *Nucl. Instrum. Methods Phys. Res. B* **372**, 312 (2008).

²⁴D. Terentyev, G. Bonny, and L. Malerba, *Acta Mater.* **56**, 3229 (2008).

²⁵D. Terentyev, P. Olsson, T. P. C. Klaver, and L. Malerba, *Comput. Mater. Sci.* **43**, 1183 (2008).

²⁶G. J. Ackland, M. I. Mendeleev, D. J. Srolovitz, S. Han, and A. V. Barashev, *J. Phys.: Condens. Matter* **16**, S2629 (2004).

²⁷M. I. Mendeleev, S. W. Han, D. J. Srolovitz, G. J. Ackland, D. Y. Sun, and M. Asta, *Philos. Mag.* **83**, 3977 (2003).

²⁸F. Willaime, C. C. Fu, M. C. Marinica, and J. D. Torre, *Nucl. Instrum. Methods Phys. Res. B* **228**, 92 (2005).

²⁹C. Domain and G. Monnet, *Phys. Rev. Lett.* **95**, 215506 (2005).

³⁰C. S. Becquart, C. Domain, A. Legris, and J.-C. van Duysen, *J. Nucl. Mater.* **280**, 73 (2000).

³¹PARCAS computer code, K. Nordlund, personal communication (May 22, 2008). The main principles of the molecular dynamics algorithms are presented in Refs. 49 and 50. The adaptive time step and electronic stopping algorithms are the same as in Ref. 51.

³²I. Mirebeau, M. Hennion, and G. Parette, *Phys. Rev. Lett.* **53**, 687 (1984).

³³P. G. Shewmon, *Diffusion in Solids* (McGraw-Hill, New York, 1963).

³⁴F. G. Djurabekova, L. Malerba, C. Domain, and C. S. Becquart, *Nucl. Instrum. Methods Phys. Res. B* **255**, 47 (2007).

³⁵D. A. Terentyev, L. Malerba, and M. Hou, *Phys. Rev. B* **75**, 104108 (2007).

³⁶T. Seletskaiia, Y. N. Osetsky, R. E. Stoller, and G. M. Stocks, *J. Nucl. Mater.* **367–370**, 355 (2007).

³⁷W. D. Wilson, Conference on Fundamental Aspects of Radiation Damage in Metals, USERDA-CONF-751006-P2, 1975 (unpublished), Vol. 1025.

³⁸N. Juslin and K. Nordlund, *J. Nucl. Mater.* **382**, 143 (2008).

³⁹J. Delley, *J. Chem. Phys.* **92**, 508 (1990).

⁴⁰DMOL is a trademark of AccelRys. Inc.

⁴¹*DMol User Guide* (Biosym, San Diego, California) v. 2.3.5 ed. (1993).

⁴²L. Laaksonen, P. Pyykkö, and D. Sundholm, *Comput. Phys. Rep.* **4**, 313 (1986).

⁴³K. Nordlund, N. Runeberg, and D. Sundholm, *Nucl. Instrum. Methods Phys. Res. B* **132**, 45 (1997).

⁴⁴J. P. Perdew, J. A. Chevary, S. H. Vosko, K. A. Jackson, M. R. Pederson, D. J. Singh, and C. Fiolhais, *Phys. Rev. B* **46**, 6671 (1992).

⁴⁵J. P. Perdew, J. A. Chevary, S. H. Vosko, K. A. Jackson, M. R. Pederson, D. J. Singh, and C. Fiolhais, *Phys. Rev. B* **48**, 4978 (1993).

⁴⁶P. E. Blöchl, *Phys. Rev. B* **50**, 17953 (1994).

⁴⁷G. Kresse and D. Joubert, *Phys. Rev. B* **59**, 1758 (1999).

⁴⁸J. Tersoff, *Phys. Rev. Lett.* **56**, 632 (1986).

⁴⁹K. Nordlund, M. Ghaly, R. S. Averback, M. Caturla, T. Diaz de la Rubia, and J. Tarus, *Phys. Rev. B* **57**, 7556 (1998).

⁵⁰M. Ghaly, K. Nordlund, and R. S. Averback, *Philos. Mag. A* **79**, 795 (1999).

⁵¹K. Nordlund, *Comput. Mater. Sci.* **3**, 448 (1995).